Interim European air quality maps for 2020

PM_{10}, NO_2 and ozone spatial estimates based on non-validated UTD data

March 2022

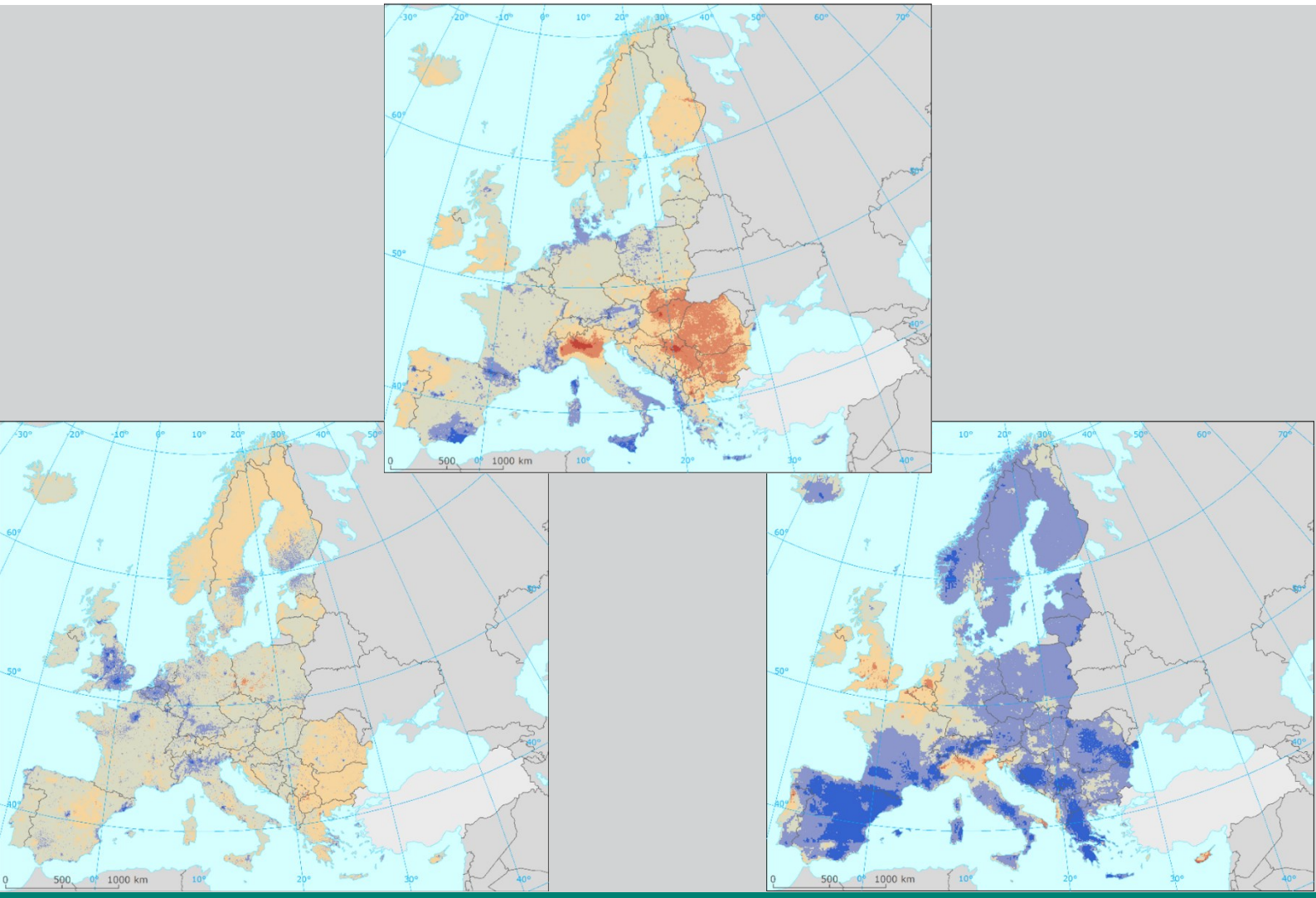

Authors:
Jan Horálek (CHMI), Markéta Schreiberová (CHMI), Leona Vlasáková (CHMI), Paul Hamer (NILU), Philipp Schneider (NILU), Jana Marková (CHMI)

ETC/ATNI consortium partners:
NILU – Norwegian Institute for Air Research, Aether Limited, Czech Hydrometeorological Institute (CHMI), EMISIA SA, Institut National de l'Environnement Industriel et des risques (INERIS), Universitat Autònoma de Barcelona (UAB), Umweltbundesamt GmbH (UBA-V), 4sfera Innova, Transport & Mobility Leuven NV (TML)

European Environment Agency
European Topic Centre on Air pollution, transport, noise and industrial pollution

Cover design: EEA
Cover pictures: Maps showing difference in concentrations of PM10 annual average (top), NO2 annual average (bottom left) and ozone indicator SOMO35 (bottom right) between 2019 and 2020. (Maps 3.2, 4.2 and 5.2 of this report).
Layout: ETC/ATNI based on EEA template

The withdrawal of the United Kingdom from the European Union did not affect the production of the report.
Data reported by the United Kingdom are included in all analyses and assessments contained herein, unless otherwise indicated.

Author(s)
Jan Horálek, Markéta Schreiberová, Leona Vlasáková, Jana Marková: Czech Hydrometeorological Institute (CHMI, Czechia)
Paul Hamer, Philipp Schneider: Norwegian Institute for Air Research (NILU, Norway)

ETC/ATNI c/o NILU
ISBN 978-82-93752-47-9

European Topic Centre on Air pollution, transport, noise and industrial pollution
c/o NILU – Norwegian Institute for Air Research
P.O. Box 100, NO-2027 Kjeller, Norway
Tel.: +47 63 89 80 00
Email: etc.atni@nilu.no
Web : https://www.eionet.europa.eu/etcs/etc-atni

Contents

Summary

The report presents interim 2020 maps for PM_{10} annual average, NO_2 annual average and the ozone indicator SOMO35. The maps have been produced based on the non-validated UTD data of the AQ e-reporting database, the CAMS Ensemble Forecast modelling data and other supplementary data. In addition to concentration maps, the inter-annual differences between the years 2019 and 2020 are presented (using the 2019 regular and the 2020 interim maps), as well as basic exposure estimates based on the interim maps. The contribution of lockdown measures connected with the Covid-19 pandemic on the change of air pollutant concentrations during the exceptional year 2020 is briefly discussed.

The population-weighted concentration of the PM_{10} annual average for 2020 for the mapped European area is estimated to be 18.1 $\mu g \cdot m^{-3}$ (which means a decrease of 0.6 $\mu g \cdot m^{-3}$ compared to 2019). For the NO_2 annual average 2020, the European-wide population-weighted concentration is estimated to be 14.0 $\mu g \cdot m^{-3}$ (i.e., it decreased by 2.9 $\mu g \cdot m^{-3}$ compared to 2019). Both for PM_{10} and NO_2, the interim results for 2020 are the lowest in the 16-year period 2005-2020. For the ozone indicator SOMO35, the population-weighted concentration for the mapped European area is estimated to be about 4 000 $\mu g \cdot m^{-3} \cdot d$ for 2020 (which means a decrease of about 480 $\mu g \cdot m^{-3} \cdot d$ compared to 2019).

The decrease in road transport, aviation and international shipping intensity during the lockdown resulted in a reduction of the NO_x emission, mainly in large cities and urbanized areas. Compared to 2019, a general decrease in NO_2 annual average concentrations is shown for 2020, as well as a decrease in values of the ozone indicator SOMO35, apart from areas with a steep NO_2 decrease. Due to the chemical processes, the decrease in NO_X resulted in an ozone increase in these areas.

The contribution of lockdown measures on the change of PM_{10} concentrations is quite complex. On the one hand, there was a decrease in emissions of suspended particles and their precursors due to decrease in transport. On the other hand, higher intensity of residential heating likely led to higher emissions of both suspended particles and their precursors.

Acknowledgements

The EEA task manager was Alberto González Ortiz.

The paper benefited from the expertise of Jana Schovánková, Pavel Kurfürst and Ondřej Vlček (CHMI, Czechia).

1 Introduction

European wide air quality annual maps have been routinely constructed under the ETC/ATNI (and the previous consortia) since 2005 (Horálek, 2021b and references therein). The mapping methodology combines monitoring data, chemical transport model results and other supplementary data using a linear regression model followed by kriging of the residuals produced from that model ('residual kriging'). Separate mapping layers (rural, urban background and urban traffic, where relevant) are created separately and subsequently merged together into the final map. In order to reflect the three steps applied, the methodology is called *Regression – Interpolation – Merging Mapping (RIMM)*. The regular maps are based on the validated air quality monitoring data as stored in the EEA's AQ e-reporting database (in the so-called E1a data set), the EMEP modelling results and other supplementary data. Due to the time schedule of the production and availability of the validated AQ measurement data and the EMEP model output, the regular RIMM maps of a year Y are typically available in May of year Y+2. Thus, the regular 2020 maps based on the validated data will be available ca. in May 2022.

This report presents the interim air quality maps for 2020, which are based on the non-validated up-to-date (UTD) measurement data (as available in the E2a data set of the AQ e-reporting database) and the CAMS Ensemble Forecast modelling results, together with other supplementary data. The reason for production of these interim maps is their earlier availability. The interim maps creation was evaluated and developed, and consequently the interim maps were recommended for regular production, see Horálek et al. (2021a, 2021b). In order to overcome an obstacle of data gaps of the E2a data in some areas, the use of so-called pseudo stations data in the areas with the lack of E2a stations was tested, based on the regression relation between the E2a data from a year Y and the validated E1a data from a year Y-1, together with the ratio of the modelling results from years Y and Y-1. The regular interim maps production was recommended for PM_{10}, NO_2 and ozone – not for $PM_{2.5}$ and not for the area of Turkey, due to the lack of the relevant monitoring data. The use of the pseudo station data in the interim mapping has been recommended for PM_{10} and NO_2. For ozone, the potential use of the pseudo data should be provisional only, until the data coverage of the E2a data is larger and the interim ozone maps might be constructed without the use of the pseudo stations.

In the report, interim 2020 maps for the PM_{10} annual average, the NO_2 annual average and the ozone indicator SOMO35 are presented. Also, the inter-annual difference between 2019 and 2020 is discussed. Next to this, population exposure estimated based on the concentration maps is briefly shown. However, in Horálek et al. (2021b) only the spatial maps have been examined, not the exposure estimates. Thus, in this report, we provide basic exposure estimates only, not the detailed information for individual countries.

Chapter 2 describes briefly the methodological aspects and documents the input data applied in the interim 2020 mapping. Chapters 3, 4, and 5 present the concentration maps and basic exposure estimates for PM_{10}, NO_2 and ozone, respectively. Chapter 6 brings the conclusions. Annex provides the technical details of the maps and their uncertainty estimates.

2 Methodology and data used maps

2.1 Methodology

2.1.1 Spatial mapping methodology

The mapping methodology used in the Regression – Interpolation – Merging Mapping method (RIMM) as routinely used in the spatial mapping under the ETC/ATNI (Horálek et. al., 2021c) consists of a linear regression model followed by kriging of the residuals from that regression model (residual kriging):

$$\hat{Z}(s_0) = c + a_1 X_1(s_0) + a_2 X_2(s_0) + \cdots + a_n X_n(s_0) + \hat{\eta}(s_0) \qquad (2.1)$$

where $\hat{Z}(s_0)$ is the estimated concentration at a point s_o,
$\hat{Z}(s_0) X_1(s_0)$ is the chemical transport model (CTM) data at point s_o,
$X_2(s_0),\ldots, X_n(s_0)$ are *n-1* other supplementary variables at point s_o,
$c, a_1, a_2,,\ldots, a_n$ are the *n+1* parameters of the linear regression model calculated based on the data at the points of measurement,
$\hat{\eta}(s_0)$ is the spatial interpolation of the residuals of the linear regression model at point s_o, based on the residuals at the points of measurement.

For different pollutants and area types (rural, urban background, and for PM_{10} and NO_2 also urban traffic), different supplementary data are used. The spatial interpolation of the regression residuals is carried out using ordinary kriging, according to

$$\hat{\eta}(s_0) = \sum_{i=1}^{N} \lambda_i \eta(s_i) \qquad \text{with } \sum_{i=1}^{N} \lambda_i = 1, \qquad (2.2)$$

where $\hat{\eta}(s_0)$ is the interpolated value at a point s_o,
N is the number of the measurement points used in the interpolation, which is fixed based on the variogram; in any case, $20 \le N \le 50$,
$\eta(s_i)$ is the residual of the linear regression model at the measurement point s_i,
$\lambda_1,\ldots, \lambda_N$ are the estimated weights based on the variogram, see Cressie (1993).

For PM_{10}, prior to linear regression and interpolation, a logarithmic transformation to measurements and CTM modelled concentrations is executed. After interpolation, a back-transformation is applied.

Separate map layers are created for rural and urban background areas on a grid at resolution of 1x1 km^2 (for PM_{10} and NO_2) and 10x10 km^2 (for ozone), and for urban traffic areas at 1x1 km^2 (for PM_{10} and NO_2). The rural background map layer is based on rural background stations, the urban background map layer on urban and suburban background stations and the potential urban traffic map layer is based on urban and suburban traffic stations. Subsequently, the separate map layers are merged into one combined final map at 1x1 km^2 resolution, according to

$$\hat{Z}_F(s_0) = \big(1 - w_U(s_0)\big) \cdot \hat{Z}_R(s_0) + w_U(s_0)\big(1 - w_T(s_0)\big) \cdot \hat{Z}_{UB}(s_0) + w_T(s_0) \cdot \hat{Z}_{UT}(s_0) \quad \text{for } PM_{10} \text{ and } NO_2$$

$$\hat{Z}_F(s_0) = \big(1 - w_U(s_0)\big) \cdot \hat{Z}_R(s_0) + w_U(s_0) \cdot \hat{Z}_{UB}(s_0) \quad \text{for ozone} \qquad (2.3)$$

where $\hat{Z}_F(s_0)$ is the resulting estimated concentration in a grid cell s_o for the final map,
$\hat{Z}_R(s_0)$, $\hat{Z}_{UB}(s_0)$ and $\hat{Z}_{UT}(s_0)$ are the estimated concentration in a grid cell s_o for the rural background, the urban background and urban traffic map layer, respectively,
$w_U(s_0)$ is the weight representing the ratio of the urban character of the grid cell s_o,
$w_T(s_0)$ is the weight representing the ratio of areas exposed to traffics in a grid cell s_o.

The weight $w_U(s_0)$ is based on the population density, while the weight $w_T(s_0)$ is based on the buffers around the roads. For details, see Horálek et al. (2021a and references therein).

2.1.2 Pseudo station data estimation

In order to supplement the E2a measurement data, which are affected by some spatial gaps, in the mapping procedure we also use data from so-called *pseudo stations.* These data are concentration estimates at the locations of stations with no E2a data for the actual year Y, but with the validated E1a data for the year Y-1. As tested in Horálek et al. (2021b), these estimates are based on the relation between E2a data from year Y and validated E1a data from year Y-1, and also the ratio of the modelling data in years Y and Y-1 is used. The estimates are calculated based on the equation

$$\hat{Z}_Y(s) = c + a_1 . Z_{Y-1}(s) + a_2 . \frac{M_Y}{M_{Y-1}} . Z_{Y-1}(s) \qquad (2.4)$$

where $\hat{Z}_Y(s)$ is the estimated concentration value at a station *s* for the year *Y*,
$Z_{Y-1}(s)$ is the measurement value at a station *s* for the year *Y-1,* based on the E1a data,
$M_Y(s)$, $M_{Y-1}(s)$ are the modelling data at a station *s* for the years *Y* and *Y-1*,
c, a_1,, a_2 are the parameters of the linear regression model calculated based on the data at the points of all stations with measurements for both *Y* and *Y-1* years.

All background stations (either classified as rural, urban or suburban) are handled together for estimating values at background pseudo stations, while all traffic stations used are applied for estimating values at traffic pseudo stations. For modelling data, CAMS Ensemble (CAMS-ENS) Forecast data (Section 2.2.2) are used.

In the interim mapping in this report, the pseudo stations have been finally used for PM_{10} and NO_2 only. For ozone, the pseudo station have not been used, dut to a large interannual variability (see Annex, Section A.3).

2.1.3 Methodology for uncertainty analysis

The uncertainty estimation of the interim maps is based on cross-validation using the E2a data. The cross-validation computes the spatial interpolation for each point of measurement from all available information except from the point in question (i.e., it withholds data of one point and then makes a prediction at the spatial location of that point). This procedure is repeated for all points of measurement in the available set. The predicted and measurement E2a values at these points are compared using statistical indicators and scatter plots. The main indicators used are root mean square error (RMSE), relative root mean square error (RRMSE) and bias (mean prediction error, MPE):

$$RMSE = \sqrt{\frac{1}{N}\sum_{i=1}^{N}\left(\hat{Z}(s_i) - Z(s_i)\right)^2} \qquad (2.5)$$

$$RRMSE = \frac{RMSE}{\bar{Z}} . 100 \qquad (2.6)$$

$$bias(MPE) = \frac{1}{N}\sum_{i=1}^{N}\left(\hat{Z}(s_i) - Z(s_i)\right) \qquad (2.7)$$

where $Z(s_i)$ is the air quality measured indicator value at the i^{th} point, *i = 1, …, N*,
$\hat{Z}(s_i)$ is the air quality estimated indicator value at the i^{th} point using other information, without the indicator value derived from the measured concentration at the i^{th} point,
$\bar{Z}$ is the mean of the indicator values $Z(s_1), …, Z(s_N)$, as measured at points *i = 1, … , N*,
N is the number of the measuring points.

Other indicators are R^2 and the regression equation parameters *slope* and *intercept*, following from the scatter plot between the predicted (using cross-validation) and the observed concentrations.

RMSE and RRMSE should be as small as possible, bias (MPE) should be as close to zero as possible, R^2 should be as close to 1 as possible, slope *a* should be as close to 1 as possible, and intercept *c* should be as close to zero as possible (in the regression equation y = a.x + c).

It should be mentioned that the uncertainty estimates are valid only for areas covered by the E2a measurements. The complete validation of the interim maps including the areas not covered by the E2a data might be done when the validated E1a data are available.

2.2 Data used

2.2.1 Air quality monitoring data

For the interim maps, we have used air quality station monitoring data coming from the E2a data set of the Air Quality e-Reporting database (EEA, 2021). The data of the up-to-date (UTD) dataflow E2a are being provided on an hourly basis from most of the EEA's member and cooperating countries.

For the purposes of the pseudo stations calculations and for the validation of the interim maps, the data of the E1a data set of the Air Quality e-Reporting database (EEA, 2020) have been used. The data of the dataflow E1a is submitted to EEA by the reporting countries every September and covers the year before the delivery. This E1a data set has been supplemented with several EMEP rural stations from the database EBAS (NILU, 2020) not reported to the Air Quality e-Reporting database.

For PM_{10} and NO_2 we use the stations classified as background (for all the three types of area, i.e., rural, suburban and urban), and also traffic for the types of area suburban and urban. For ozone, we use only data from stations classified as background (for the three types of area). In the mapping, rural background stations are used for the rural layer, urban and suburban stations for the urban background layer and urban and suburban traffic stations for the urban traffic layer (Section 2.1).

The following pollutants and aggregations are considered:

PM_{10} – annual average [$\mu g \cdot m^{-3}$], years 2019 (E1a) and 2020 (E2a),
Ozone – SOMO35 [$\mu g \cdot m^{-3} \cdot d$], years 2019 (E1a) and 2020 (E2a),
NO_2 – annual average [$\mu g \cdot m^{-3}$], years 2019 (E1a) and 2020 (E2a).

Tables 2.1 and 2.2 show the number of the stations used in the interim mapping. In the RIMM mapping (as described in Section 2.1) of the year 2020, E2a 2020 stations are used, together with pseudo stations derived from E1a stations of the year 2019. The pseudo stations are located at the places of the E1a 2019 stations with no E2a data for year 2020 (labelled "For pseudo 2020"). The rest of the E1a 2019 stations (with both E1a data for 2019 and E2a data for 2020, labelled "For regression") are used for estimation of the parameters of the linear regression for the pseudo stations calculation (see Eq. 2.4).

Table 2.1: Number of stations used in interim mapping 2020 for each station type, for PM_{10} (left) and NO_2 (right)

Station type	PM_{10}				NO_2			
	E1a 2019			E2a 2020	E1a 2019			E2a 2020
	Total	For regression	For pseudo 2020	Mapping 2020	Total	For regression	For pseudo 2020	Mapping 2020
Rural background	381	215	166	230	466	340	126	357
Urban/suburb. backgr.	1452	774	678	820	1411	1057	354	1113
Urban/suburb. traffic	775	494	281	508	1101	670	431	689

Table 2.2: Number of stations used in interim mapping 2020 for each station type, for ozone

Station type	Ozone			
	E1a 2019			E2a 2020
	Total	For regression	For pseudo 2020	Mapping 2020
Rural background	549	469	-	487
Urban/suburb. backgr.	1216	981	-	1014

Maps A.1-A.3 of Annex show the spatial distribution of the rural, urban/suburban background and urban/suburban traffic stations used in the interim 2020 mapping (in green and orange), for different pollutants. In all figures, the true stations (in green) and the pseudo stations (in orange) are distinguished.

2.2.2 Chemical transport modelling (CTM) data

CAMS Ensemble Forecast Modelling Data

We use the CAMS Ensemble Forecast data as provided by the Copernicus Atmosphere Monitoring Service (CAMS) at a regional scale over Europe. The European regional production consists of an ensemble of nine air quality models run operationally. For further details of individual models, see Marécal et al. (2015). The models provide (together with other products) a 72-hour forecast made available at 07:00 UTC the day of the forecast. The forecast data product is available on an hourly time resolution and at a spatial resolution of 0.1° x 0.1°, i.e., ca. 10x10 km^2. Each model forecast is combined into an ensemble forecast by taking the median of all nine models.

The forecast products are available at hourly intervals and have a spatial resolution of 0.1 × 0.1°. All the models used in the CAMS ensemble products were run using the TNO-MACC emissions representative of 2011 (Kuenen et al., 2014) and the meteorology (i.e., the weather forecast) provided by the European Centre for Medium Range Weather Forecasts (ECMWF) operationally.

We have downloaded the CAMS Ensemble Forecast data for 2019 and 2020 from the CAMS data archive (http://www.regional.atmosphere.copernicus.eu/?category=data_access). The modelling data have been downloaded in NetCDF format.

All modelling data have been aggregated into the annual statistics and converted into the reference EEA 1x1 km^2 (for PM and NO_2) and 10x10 km^2 (for ozone) grids. The pollutants and parameters used are the same as for the monitoring data.

2.2.3 Other supplementary data

Other supplementary data used are similar as in regular maps creation, Horálek et al. (2021c).

Altitude

We use the altitude data field (in m) of Global Multi-resolution Terrain Elevation Data 2010 (GMTED2010), with an original grid resolution of 15x15 arcseconds coming from U.S. Geological Survey Earth Resources Observation and Science, see Danielson and Gesch (2011). The data were converted into the EEA reference grids in 1x1 km^2 and 10x10 km^2 resolutions. Next to this, another aggregation has been executed based on the 1x1 km^2 grid cells, i.e., the floating average of the circle with a radius of 5 km around all relevant grid cells.

Meteorological data

The meteorological data used are the ECWMF data extracted from the CDS (Climate Data Store, https://cds.climate.copernicus.eu/cdsapp#!/home). Specifically, the hourly data of the reanalysed

data set ERA5-Land in 0.1°x0.1° resolution have been used. The hourly data have been derived into the parameters needed, aggregated into the annual statistics and converted into the reference EEA 1x1 km^2 (for PM and NO_2) and 10x10 km^2 (for ozone) grids. For details, see Horálek et al. (2021c). Meteorological parameters used are *wind speed* (annual mean for 2020, in $m.s^{-1}$), *relative humidity* (annual mean for 2020, in percent) and *surface net solar radiation* (annual mean of daily sum for 2020, in $MWs.m^{-2}$).

Satellite data

Data from the TROPOspheric Monitoring Instrument (TROPOMI) onboard of the Sentinel-5 Precursor satellite was used. Their spatial resolution is approximately 5.5 km by 3.5 km. The product used is the S5P_OFFL_L2__NO2 product (van Geffen et al., 2020) and it provides the tropospheric vertical column density of nitrogen dioxide (NO_2), i.e., a vertically integrated value over the entire troposphere. All overpasses for a specific day were then mosaicked and gridded into the reference EEA 1x1 km^2 grid in the ETRS89 / ETRS-LAEA (EPSG 3035) projection. The daily gridded files were subsequently averaged to an annual mean.

Land cover

CORINE Land Cover 2018 – grid 100 x 100 m^2, Version 2020_20 (EU, 2020) is used. Like in Horálek et al. (2021c), the 44 CLC classes have been re-grouped into the 8 more general classes. In this paper, we use five of these general classes, namely high density residential areas (HDR), low density residential areas (LDR), agricultural areas (AGR), natural areas (NAT), and traffic areas (TRAF). For details, see Horálek et al. (2021b). Two aggregations are used, i.e., into 1x1 km^2 grid and into the circle with radius of 5 km. The aggregated grid value represents for each general class the total area of this class as percentage of the total area of the 1x1 km^2 square or the circle with radius of 5 km.

Population density and Road data

Population density (in $inhabitants.km^{-2}$, census 2011) is based on Geostat 2011 grid dataset (Eurostat, 2014). For regions not included in the Geostat 2011 dataset we use as alternative sources JRC and ORNL data. For details, see Horálek et al. (2021b).

GRIP vector road type data is used (Meijer et al., 2018). Based on these data (i.e., buffers around the roads), traffic map layers (Section 2.1) are merged into the final maps (Horálek et al., 2021b).

3 PM_{10}

Map 3.1 presents the interim map for the PM_{10} annual average 2020, as the result of interpolation and merging of the separate map layers as described in Annex, Section A.1. Red and purple areas indicate exceedances of the limit value (LV) of 40 µg·m^{-3}.

Map 3.1: Interim concentration map of PM_{10} annual average, 2020, RIMM methodology using E2a (UTD) measurement data, pseudo data and CAMS-ENS Forecast model output

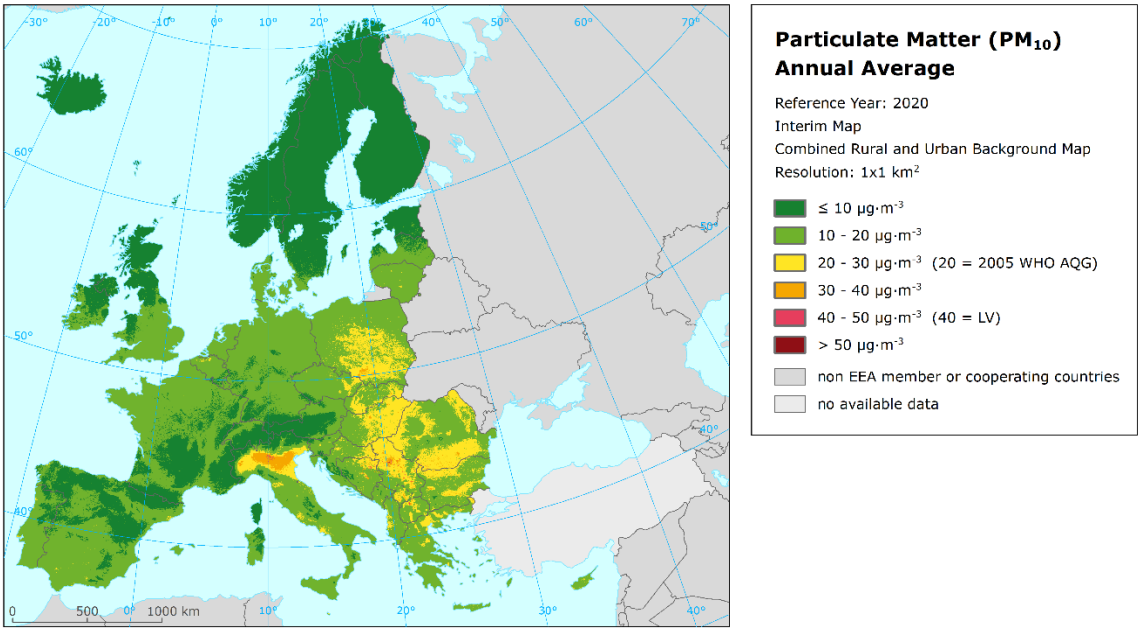

The map shows annual LV exceedances only in Naples and small area in the Po Valley and in small urban areas around the Balkan cities (North Macedonia, Serbia and Croatia). The Po Valley is the area with the highest PM_{10} concentrations reaching 30-40 µg.m^{-3}. Most of the south-eastern area plus Hungary, Slovakia and Poland shows PM_{10} levels below 30 µg·m^{-3}. Annual average PM_{10} concentration below 20 µg.m^{-3} or even 10 µg.m^{-3} (Scandinavia and mountainous area) can be found in the rest of Europe.

Map 3.2 shows the inter-annual difference of PM_{10} annual average between 2019 and 2020 (using the 2019 regular and the 2020 interim maps). Orange to red areas show an increase of PM_{10} concentration in 2020, while blue areas show a decrease.

Compared to 2019, the highest increase in PM_{10} concentration is shown in the Po Valley, Slovakia, Hungary, Romania, Serbia, North Macedonia and parts of Greece, Croatia and Slovenia. On the other hand, the deepest decrease is shown in parts of Italy, Spain, France, Austria, Poland and Denmark.

The contribution of lockdown measures connected with the SARS-CoV-2 (severe acute respiratory virus coronavirus 2) pandemic from mid-March 2020 on the change of PM_{10} concentration is quite complicated due to the different composition of PM_{10} and PM_{10} gaseous precursor emission sources and strong dependency of PM_{10} concentrations on dispersion and meteorological conditions. On the one hand, there was a decrease in emissions of suspended particles and nitrogen oxides (precursors of secondary suspended particles) due to decrease in transport. On the other hand, the likely higher intensity of heating due to the population remaining in their homes during lockdown led to higher emissions of both suspended particles and their precursors.

Map 3.2: Difference concentrations between 2019 and 2020 (based on the interim map) for PM_{10} annual average

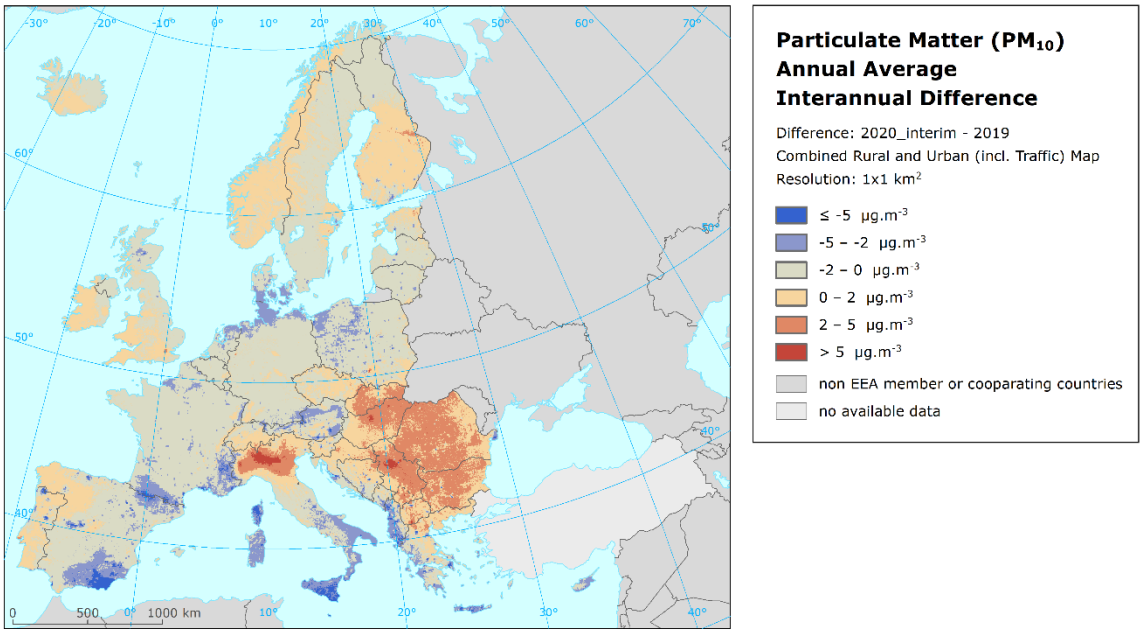

Based on the mapping results and the population density data, the population exposure estimates have been calculated. Table 3.1 gives the population frequency distribution for a limited number of exposure classes and the population-weighted concentration for large European regions, for EU-27 and for the total mapping area.

The table presents the country grouping of the following large regions: 1) Northern Europe: Denmark, Estonia, Finland, Latvia, Lithuania, Norway, and Sweden, 2) North-western Europe: Belgium, France north of 45 degrees latitude, Iceland, Ireland, Luxembourg, the Netherlands, and the United Kingdom, 3) Central and South-Eastern Europe : Austria, Bulgaria, Czechia, Germany, Hungary, Liechtenstein, Poland, Romania, Slovakia and Switzerland, and 4) Southern Europe: Albania, Bosnia and Herzegovina, Croatia, Cyprus, France south of 45 degrees latitude, Greece, Italy, Malta, Monaco, Montenegro, North Macedonia, Portugal, San Marino, Serbia (including Kosovo under the UN Security Council Resolution 1244/99), Slovenia, and Spain.

Table 3.1: Population exposure and population-weighted concentration, PM_{10} annual average, 2020, based on interim map

Area	Population [inhbs·1000]	PM_{10} – annual average, exposed population, 2019 [%]						PM_{10} ann. avg.
		< 10	10 - 20	20 - 30	30 - 40	40 - 50	> 50	Pop. weighted
Northern Europe		44.8	52.7	2.6				11.3
North-western Europe		3.3	93.5	3.2				15.4
Central & South-eastern Europe		2.4	61.6	29.3	6.6	0.1		18.6
Southern Europe		1.7	53.2	31.0	12.5	1.6	0.0	21.2
Total		**5.0**	**67.2**	**21.1**	**6.2**	**0.5**	**0.0**	**18.1**
EU-27		**4.6**	**65.5**	**23.4**	**6.3**	**0.2**		**18.2**

Note: The percentage value "0.0" indicates that an exposed population exists, but it is small and estimated to be less than 0.05 %. Empty cells mean no population in exposure.

Based on the interim map, it is estimated that 0.5 % of population living in the considered (i.e., mapped) European area has been exposed to concentrations exceeding the EU annual limit value (ALV) of 40 µg·m^{-3} (0.2 % for the EU-27). About 28 % of the considered European population (and 30 % of the EU-27 population) has been exposed to annual average concentrations above the Air Quality Guideline of 20 µg·m^{-3} recommended by the World Health Organization in 2005 (WHO, 2005)[1]. The population-weighted concentration of the PM_{10} annual average for 2020 for the considered European countries and for EU-27 is estimated to be about 18 µg·m^{-3}.

Figure 3.1 shows, for the whole mapped area, the population frequency distribution for exposure classes of 1 µg·m^{-3}. The highest population frequency is found for classes between 13 and 18 µg·m^{-3}. A quite continuous decline of population frequency is visible for classes between 20 and 30 µg·m^{-3} and beyond 35 µg·m^{-3}.

Figure 3.1: Population frequency distribution, PM_{10} annual average 2020, based on interim map. The 2005 WHO´s AQ Guideline (20 µg·m^{-3}) is marked by the green line, the annual limit value (40 µg·m^{-3}) is marked by the red line.

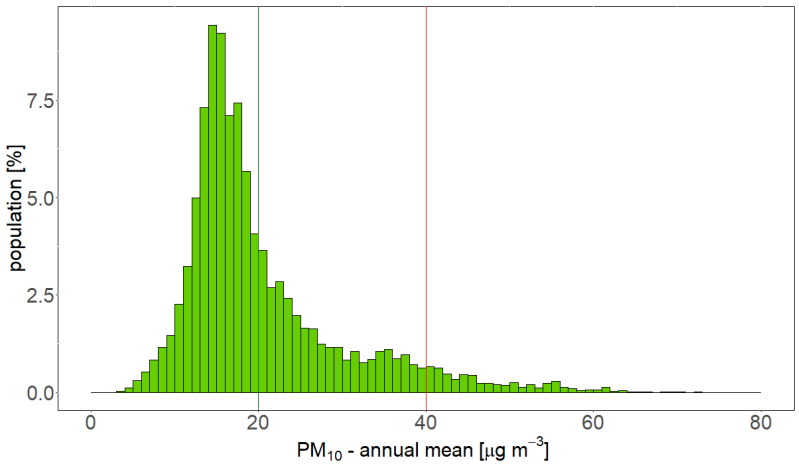

Note: Apart from the population distribution shown in graph, it was estimated that 0.01 % of population lived in areas with PM_{10} annual average concentration in between 80 and 95 µg·m^{-3}.

For changes in the population-weighted concentrations of the PM_{10} annual average in the period 2005-2019, see Figure 3.2. The PM concentrations show a steady decrease of almost 0.7 µg·m^{-3} per year for PM_{10} annual average. One can see that the interim results for 2020 are the lowest in the 16-year period.

[1] Be aware that during the finalizing of this report, WHO introduced its new Air Quality Global Guidelines (WHO, 2021). Due to time reasons, we do not include in this report the assessments against these 2021 WHO AQG.

Figure 3.2: Population-weighted concentration of PM_{10} annual average in 2005-2020, based on both the old (blue) and the updated (red) mapping methodology, where available, and with 2020 interim results

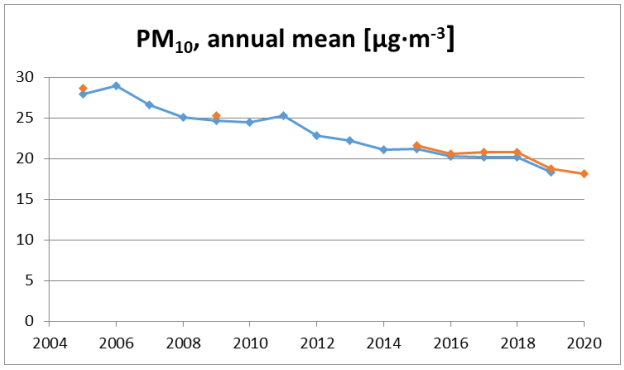

4 NO_2

Map 4.1 presents the interim map for the NO_2 annual average 2020, as the result of interpolation and merging of the separate map layers as described in Annex, Section A.2. Red and purple areas indicate exceedances of the limit value (LV) of 40 µg·m^{-3}. Dark green areas indicate concentrations below 10 µg·m^{-3} (being the new 2021 WHO AQG level).

The areas where the annual limit value of 40 µg·m^{-3} for NO_2 was exceeded include urbanized parts of some large cities, particularly Milan and Naples. Some other cities show NO_2 levels above 30 µg·m^{-3}, e.g. in Spain, France, Italy, Great Britain and Romania. Most of the European area shows NO_2 levels below 10 µg·m^{-3}. Some larger areas above 10 µg·m^{-3} can be found in the Po Valley, the Benelux, the German Ruhr region, in central and southern England, in the Île de France region and around Rome.

Map 4.1: Interim concentration map of NO_2 annual average, 2020, RIMM methodology using E2a (UTD) measurement data, pseudo data and CAMS-ENS Forecast model output

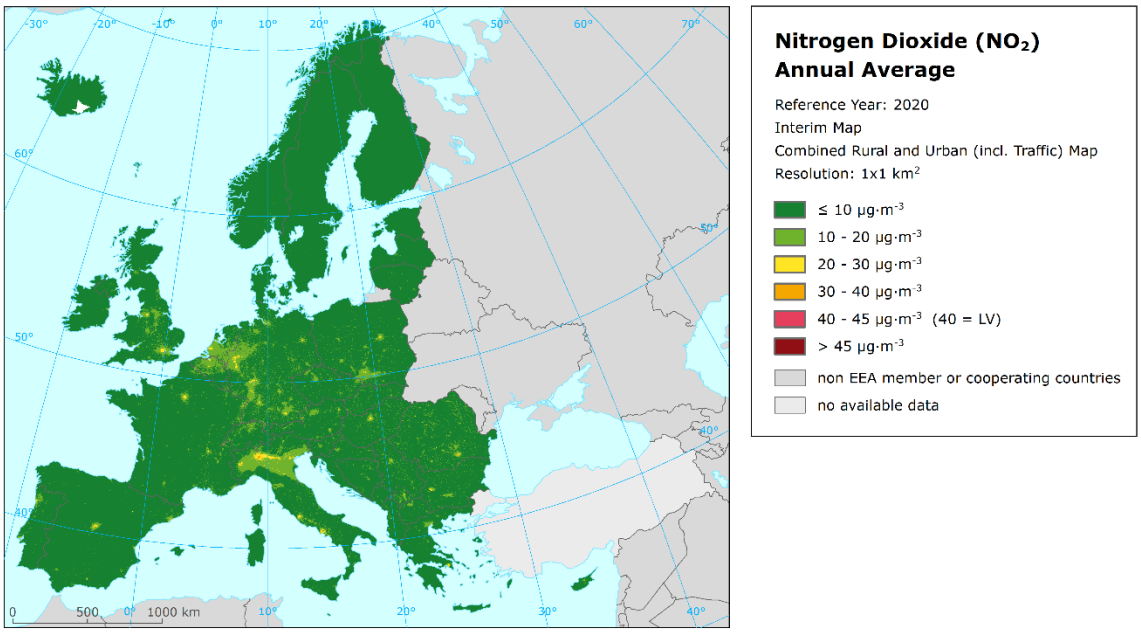

Map 4.2 shows the inter-annual difference of NO_2 annual average between 2019 and 2020 (using the 2019 regular and the 2020 interim maps). Orange to red areas show an increase of PM_{10} concentration in 2020, while blue areas show a decrease.

In comparison to 2019, general decrease in NO_2 annual concentration is shown. The NO_2 concentration (in terms of annual average) shows a decrease of more than 5 $\mu g \cdot m^{-3}$ per year in areas of London, Paris, Rome, Milano, Madrid, Barcelona. The decrease up to 5 $\mu g \cdot m^{-3}$ has been observed in some areas of the United Kingdom, Benelux, the Po Valley and in the other European cities. One of the reason for it is the lockdown measures connected with the SARS-CoV-2 pandemic. The decrease in the road transport, aviation and international shipping intensity during the lockdown resulted in the reduction of the emission and ambient air concentrations of NO_X, mainly in large cities and urbanized parts (EEA, 2020). Some European areas show no change or even mild increase in annual NO_X concentrations (northern Europe and south-eastern Europe states).

Map 4.2: Difference concentrations between 2019 and 2020 (based on the interim map) for NO_2 annual average

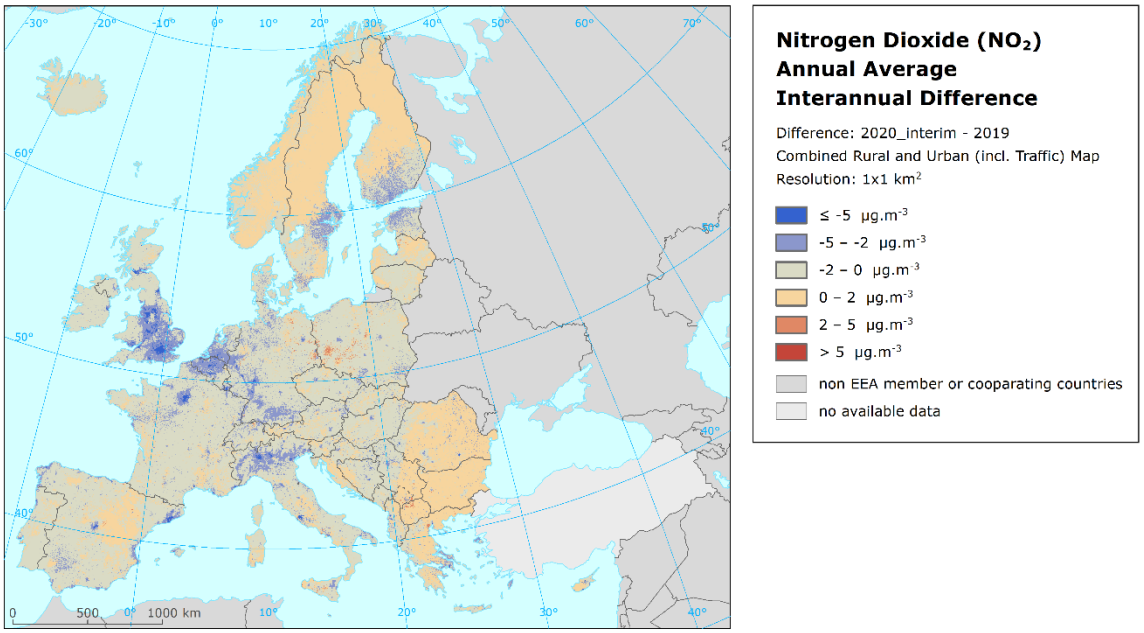

Based on the mapping results and the population density data, the population exposure estimate has been calculated. Table 4.1 gives the population frequency distribution for a limited number of exposure classes and the population-weighted concentrations for large European regions, for EU-27 and for the total mapping area.

Table 4.1: Population exposure and population-weighted concentration, NO_2 annual average, 2020, based on interim map

Area	Population [inhbs·1000]	NO_2 – annual average, exposed population, 2020 [%]						NO_2 ann. avg.
		< 10	10 - 20	20 - 30	30 - 40	40 - 45	> 45	Pop. weighted
Northern Europe		76.3	23.1	0.6				7.4
North-western Europe		29.1	57.2	12.2	1.2	0.2		13.4
Central & South-eastern Europe		21.7	63.0	13.6	1.6	0.0	0.1	14.6
Southern Europe		25.9	52.4	18.0	3.5	0.2		15.0
Total		**28.3**	**55.7**	**13.8**	**2.0**	**0.1**	**0.0**	**14.0**
EU-27		**29.0**	**54.0**	**14.5**	**2.3**	**0.2**	**0.0**	**14.1**

Note: The percentage value "0.0" indicates that an exposed population exists, but it is small and estimated to be less than 0.05 %. Empty cells mean no population in exposure.

Based on the interim map, it is estimated that ca. 0.1 % of population of the considered European area (and 0.2 % of the EU-27 population) has been exposed to concentrations exceeding the EU annual limit value (ALV) of 40 µg·m^{-3}. 72 % of the total area population (and 71 % of the EU-27 population) has been exposed to concentrations exceeding 10 µg·m^{-3} (being the new 2021 WHO AQG level). The population-weighted concentration of the NO_2 annual average for 2020 for the considered European population and for the EU-27 is estimated to be about 14 µg·m^{-3}

Figure 4.1 shows, for the whole mapped area, the population frequency distribution for exposure classes of 1 µg·m^{-3}. One can see the highest population frequency for classes between 10 and 15 µg·m^{-3}, continuous decline of population frequency for classes between 15 and 25 µg·m^{-3} and continuous mild decline of population frequency for classes between 25 and 50 µg·m^{-3}.

Figure 4.1: Population frequency distribution, NO_2 annual average 2020, based on interim map. The annual limit value (40 µg·m^{-3}) is marked by the red line.

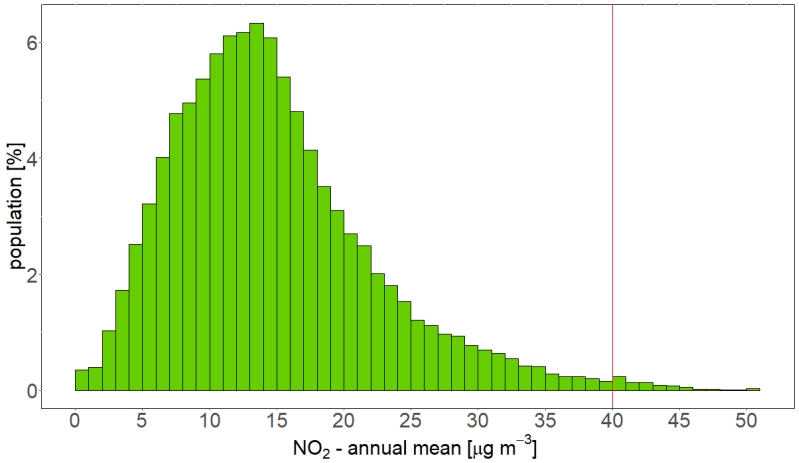

For changes in the population-weighted concentrations of the NO_2 annual average in the period 2005-2020, see Figure 4.2. The NO_2 concentration (in terms of annual average) shows a decrease of about 0.5 µg·m^{-3} per year. One can see that the interim results for 2020 are the lowest in the 16-year period.

Figure 4.2: Population-weighted concentration of NO_2 annual average in 2005-2020, where available, and with 2020 interim results

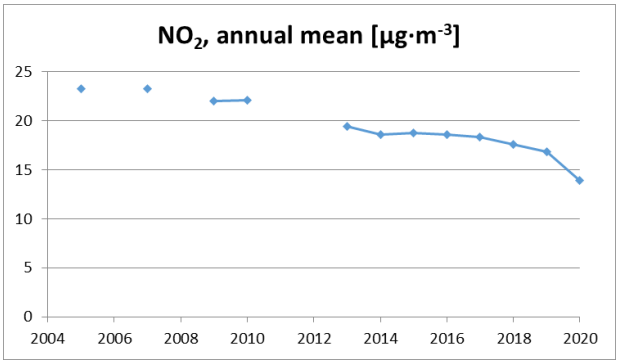

5 Ozone

Map 5.1 presents the interim 2020 map for SOMO35 as a result of merging separate rural and urban interpolated map layers as described in Annex, Section A.3. Red and purple areas show values above 8 000 µg·m^{-3}·d, while the orange areas show values above 6 000 µg·m^{-3}·d.

Generally the southern parts of Europe show higher ozone SOMO35 concentrations than the northern parts. Higher levels of ozone also occur more frequently in mountainous areas south of 50 degrees latitude than in lowlands.

Map 5.1: Interim concentration map of ozone indicator SOMO35, 2020, RIMM methodology using E2a (UTD) measurement data and CAMS-ENS Forecast model output

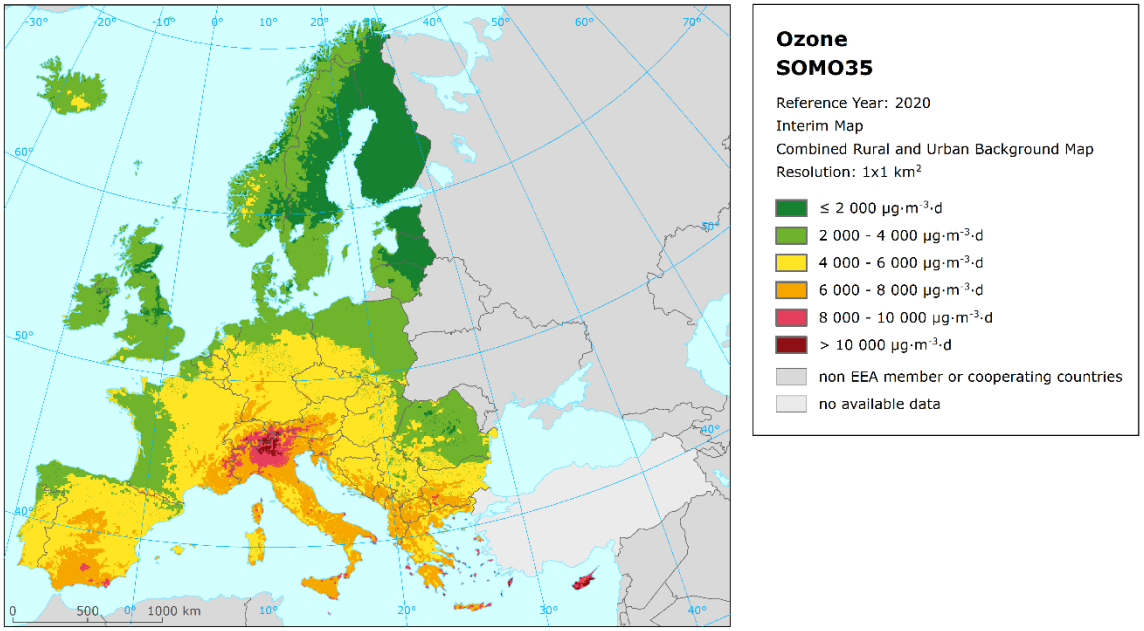

Map 5.2 shows the inter-annual difference of the ozone indicator SOMO35 between 2019 and 2020 (using the 2019 regular and the 2020 interim maps). Orange to red areas show an increase of PM_{10} concentration in 2020, while blue areas show a decrease.

The annual mean temperature shows that 2020 was the warmest year on record (since 1950), at more than 1.6°C above average. However, it was the cool seasons that were particularly warm, with both winter and autumn being the warmest on record. Although summer 2020 as a whole was not exceptionally warm, there were several significant episodes affecting different regions each month. Nevertheless, the heatwaves of 2020 were not as intense, widespread or long-lived as others in recent years. Moreover, after a relatively wet June, July to September had near-average precipitation amounts (ECMWF, 2020). To conclude, these meteorological factors, were less favourable for the formation of ozone than in 2019.

As a result, most of Europe show a quite high decrease in 2020 compared to 2019, with the exception of areas in the United Kingdom, Benelux, Île de France region and the Po Valley. Nevertheless, in these mentioned areas, the steep decrease in NO_2 concentrations has been showed (see Map 4.2). Tropospheric ozone formation occurs when NO_x and volatile organic compounds (VOCs) react in the atmosphere in the presence of sunlight (Seinfeld and Pandis, 1998). As NO_X is a precursor of ozone, change in NO_2 (part of NO_x) concentrations can indicate change in ozone concentration. It has been stated by a few authors that decrease in NO_X concentrations due to lockdown measures can result in ozone concentrations increase, especially in cities and urban areas

(e.g. Brancher 2021, Sicard et al. 2020, Tobías et al. 2020). The study by Brancher et al. (2021), which deals with the change in ozone concentrations during the SARS-CoV-2 pandemic, points to an increase in ground-level ozone concentrations due to a decrease in NO_X emissions during lockdowns and subsequent decreased ground-level ozone titration with nitric oxide. According to Sicard et al. (2020), the NOx reduction during the lockdown higher than the VOCs reduction possibly led to higher VOC-NOx ratio, which enhanced the ozone production. Sicard et al. (2020) also even points to the possibility of increasing VOC (i.e. other ozone precursor) emissions during lockdowns due to home and garden activities (cleaning, grilling, biomass combustion).

Map 5.2: Difference concentrations between 2019 and 2020 (based on the interim map) for ozone indicator SOMO35

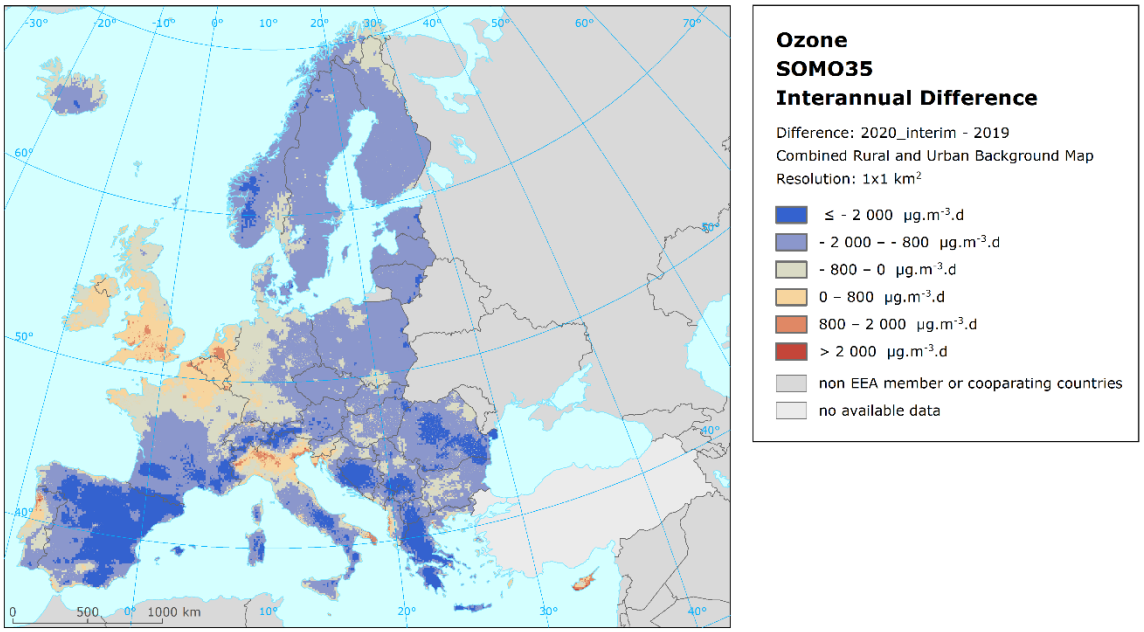

Based on the mapping results and the population density data, the population exposure estimate has been calculated. Table 5.1 gives the population frequency distribution for a limited number of exposure classes and the population-weighted concentration for large European regions, for EU-27 and for the total mapping area.

Table 5.1: Population exposure and population-weighted concentration, ozone indicator SOMO35, 2020, based on interim map

Area	Population [inhbs·1000]	Ozone - SOMO35, exposed population, 2020 [%]						Ozone - SOMO35
		< 2000	4000	6000	8000	10000	> 10000	Pop. weighted
Northern Europe		75.5	24.5	0.0				1 719
North-western Europe		16.3	59.7	23.6	0.4	0.0		3 211
Central & South-eastern Europe		3.1	50.6	45.3	0.9	0.1	0.0	3 862
Southern Europe		0.7	23.4	45.9	22.0	7.5	0.5	5 277
Total		**10.3**	**43.0**	**36.9**	**7.3**	**2.4**	**0.1**	**3 997**
EU-27		**6.6**	**40.2**	**41.6**	**8.6**	**2.8**	**0.2**	**4 252**

Note: The percentage value "0.0" indicates that an exposed population exists, but it is small and estimated to be less than 0.05 %. Empty cells mean no population in exposure.

Based on the interim map, it is estimated that almost 10 % of the considered European population (12 % of the EU-27) lived in areas with SOMO35 values above 6 000 µg·m^{-3}·d. The population-

weighted concentration of the SOMO35 for 2020 for the considered European population is estimated to be about 4 000 µg·m^{-3}·d (4 300 µg·m^{-3}·d for the EU27).

Figure 5.1 shows, for the whole mapped area, the frequency distribution of SOMO35 for population exposure classes of 250 µg·m^{-3}·d. The highest frequencies are found for classes between 3 000 and 5 000 µg·m^{-3}·d. One can see a decline of population frequency for exposure classes between 5 000 and 8 000 µg·m^{-3} and a continuous mild decline of population frequency for classes above 8 000 µg·m^{-3}·d.

Figure 5.1: Population frequency distribution, ozone indicator SOMO35, 2020, based on interim map

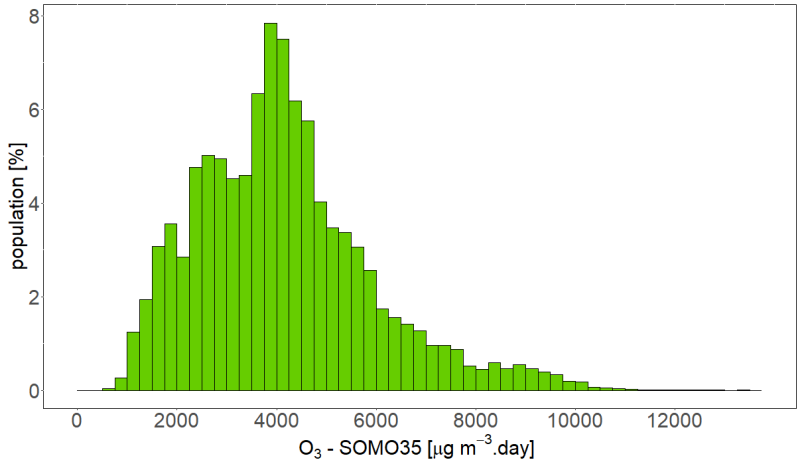

For changes in the population-weighted concentrations in the period 2005-2020, see Figure 4.2. No trend is observed for the SOMO35, due to the year-to-year variability.

Figure 5.2: Population-weighted concentration of the ozone indicator SOMO35 in 2005-2020, with 2020 interim results

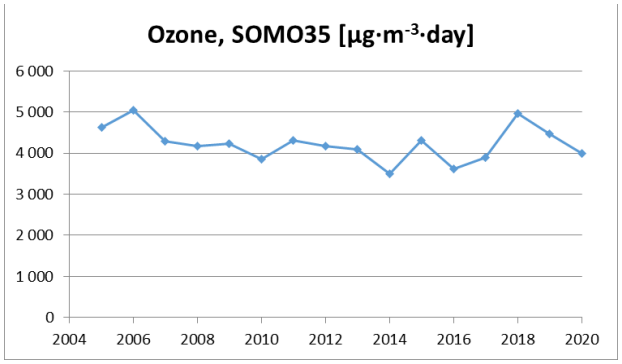

6 Conclusions

The report presents the interim 2020 maps for PM_{10} annual average, NO_2 annual average and the ozone indicator SOMO35. The maps have been produced based on the non-validated E2a (UTD) data of the AQ e-reporting database, the CAMS Ensemble Forecast modelling data and other supplementary data. Together with the concentration maps, the inter-annual differences between years 2019 and 2020 are presented (using the 2019 regular and the 2020 interim maps), as well as basic exposure estimates based on the interim maps. The contribution of lockdown measures connected with the SARS-CoV-2 on the change of air pollutant concentrations during the exceptional year 2020 is briefly discussed.

For PM_{10}, annual limit value (LV) of 40 $\mu g \cdot m^{-3}$ exceedances are shown only in Naples and small area in the Po Valley and in small urban areas around the Balkan cities (North Macedonia, Serbia and Croatia). 0.5 % of the considered European population is exposed to levels above the EU annual LV; almost 28 % of the considered European population is exposed to levels above the 2005 WHO PM_{10} Air Quality Guideline of 20 $\mu g \cdot m^{-3}$. The contribution of lockdown measures on the change of PM_{10} concentrations is quite complicated. On the one hand, there was a decrease in emissions of suspended particles and nitrogen oxides (precursors of secondary suspended particles) due to decrease in transport. On the other hand, the likely higher intensity of heating due to the population remaining in their homes during lockdown led to higher emissions of both suspended particles and their precursors.

In the case of NO_2, the annual LV of 40 $\mu g \cdot m^{-3}$ for NO_2 was exceeded in urbanized parts of some large cities, particularly Milan and Naples. It is estimated that ca. 0.1 % of the considered European population is exposed to levels above the EU annual LV. In comparison to 2019, general decrease in NO_2 annual concentrations is shown. The decrease in the road transport, aviation and international shipping intensity during the lockdown resulted in the reduction of the emission and ambient air concentrations of NO_X, mainly in large cities and urbanized areas. The population-weighted concentration of the NO_2 annual average was the lowest in the 16-year period 2005-2020.

For ozone, most of Europe show a quite high decrease in 2020 compared to 2019, with the exception of areas in the United Kingdom, Benelux, Île de France region and the Po Valley. Nevertheless, in these mentioned areas, the steep decrease in NO_2 concentrations has been showed. Due to the chemical processes, the decrease in NO_X concentrations due to lockdown measures can result in ozone concentrations increase, especially in cities and urban areas.

Uncertainty estimates based on the cross-validation of the E2a data have been performed for all interim maps. However, these uncertainty estimates are valid for areas covered by the E2a measurements only. The complete validation of the interim maps including the areas not covered by the E2a data should be done when the validated E1a data for 2020 are available.

In the report, only a brief population exposure for large European regions and the total mapped area has been presented, as the population exposure based on the interim maps has not been validated yet. It is recommended to examine the more detailed exposure estimates (i.e., for particular European countries) based on the interim maps and to validate them against the exposure estimates based on regular maps.

References

Brancher, M., 2021. 'Increased ozone pollution alongside reduced nitrogen dioxide concentrations during Vienna's first COVID-19 lockdown: Significance for air quality management', *Environmental Pollution* 284, p. 117153 (https://doi.org/10.1016/j.envpol.2021.117153) accesed 16 February 2021.

Cressie, N., 1993, *Statistics for spatial data,* Wiley series, New York.

Danielson, J. J. and Gesch, D. B., 2011, *Global multi-resolution terrain elevation data 2010 (GMTED2010)*, U.S. Geological Survey Open-File Report, pp. 2011-1073 (https://pubs.er.usgs.gov/publication/ofr20111073) accessed 19 November 2020.

ECMWF, 2020, *European State of the Climate 2020*, Copernicus Climate Change Service, Full report (https://climate.copernicus.eu/ESOTC/2020) accessed 13 October 2021.

EEA, 2020. Air quality in Europe – 2020. EEA Report 09/2020. European Environment Agency. (https://www.eea.europa.eu/publications/air-quality-in-europe-2020-report).

Eurostat, 2014, *GEOSTAT 2011 grid dataset. Population distribution dataset* (http://ec.europa.eu/eurostat/web/gisco/geodata/reference-data/population-distribution-demography) accessed 26 August 2020.

Horálek, J., et al., 2021a, *Potential use of CAMS modelling results in air quality mapping under ETC/ATNI*, Eionet Report ETC/ATNI 2019/17 (https://doi.org/10.5281/zenodo.4627762) accessed 15 June 2021.

Horálek, J., et al., 2021b, *European air quality interim mapping under ETC/ATNI*, Eionet Report ETC/ATNI 2020/11 (https://doi.org/10.5281/zenodo.5564555) accessed 12 October 2021.

Horálek, J., et. al., 2021c, *European air quality maps for 2019*, Eionet Report ETC/ATNI 2021/1, *in preparation*.

Kuenen, J. J. P., et al., 2014, 'TNO-MACC_II emission inventory; a multi-year (2003--2009) consistent high-resolution European emission inventory for air quality modelling', *Atmospheric Chemistry and Physics*, 14, pp. 10963–10976 (https://doi.org/10.5194/acp-14-10963-2014) accesed 16 February 2021.

Marécal, V., et al., 2015, 'A regional air quality forecasting system over Europe: The MACC-II daily ensemble production', *Geoscientific Model Development*, 8, pp. 2777–2813 (https://doi.org/10.5194/gmd-8-2777-2015) accesed 16 February 2021.

Meijer, J. R., et al., 2018, 'Global patterns of current and future road infrastructure', *Environmental Research Letters*, 13 0640, (https://doi.org/10.1088/1748-9326/aabd42) accesed 10 June 2019.

NILU, 2021, *EBAS, database of atmospheric chemical composition and physical properties* (http://ebas.nilu.no) accessed 8 April 2021.

Seinfeld, J. H., Pandis, S. N., 2006. *Atmospheric chemistry and physics: from air pollution to climate change*, 2nd edition, New York: John Wiley & Sons, Inc. ISBN 978-0-471-72017-1.

Sicard, P., et al., 2020. 'Amplified ozone pollution in cities during the COVID-19 lockdown', *Science of The Total Environment* 735, p. 139542 (https://doi.org/10.1016/j.scitotenv.2020.139542) accessed 19 August 2021 .

Tobías, A., et al., 2020. 'Changes in air quality during the lockdown in Barcelona (Spain) one month into the SARS-CoV-2 epidemic', *Science of Total Environment* 726, p. 138540. (https://doi.org/10.1016/j.scitotenv.2020.138540) accesed 19 August 2021.

van Geffen, J., et al., 2020, 'S5P TROPOMI NO_2 slant column retrieval: Method, stability, uncertainties and comparisons with OMI', *Atmospheric Measurement Techniques* 13, pp. 1315–1335 (https://doi.org/10.5194/amt-13-1315-2020) accessed 30 August 2021.

Annex
Technical details and uncertainties of interim maps

This Annex presents the maps showing the air quality stations used for the mapping of 2020 interim maps, as well as the technical details on the map creation. Furthermore, uncertainty estimates of the maps are given.

A.1 PM_{10}

This sections present the technical details and uncertainty estimates of the PM_{10} annual average interim map as presented in Map 3.1.

Maps of measurement stations used for mapping

Map A.1 shows the spatial distribution of the rural, urban/suburban background and urban/suburban traffic stations used in the interim mapping of PM_{10} annual average 2020. In all figures, the true stations (in green) and the pseudo stations (in orange) are distinguished.

Map A.1: Spatial distribution of PM_{10} stations used in interim mapping, 2020

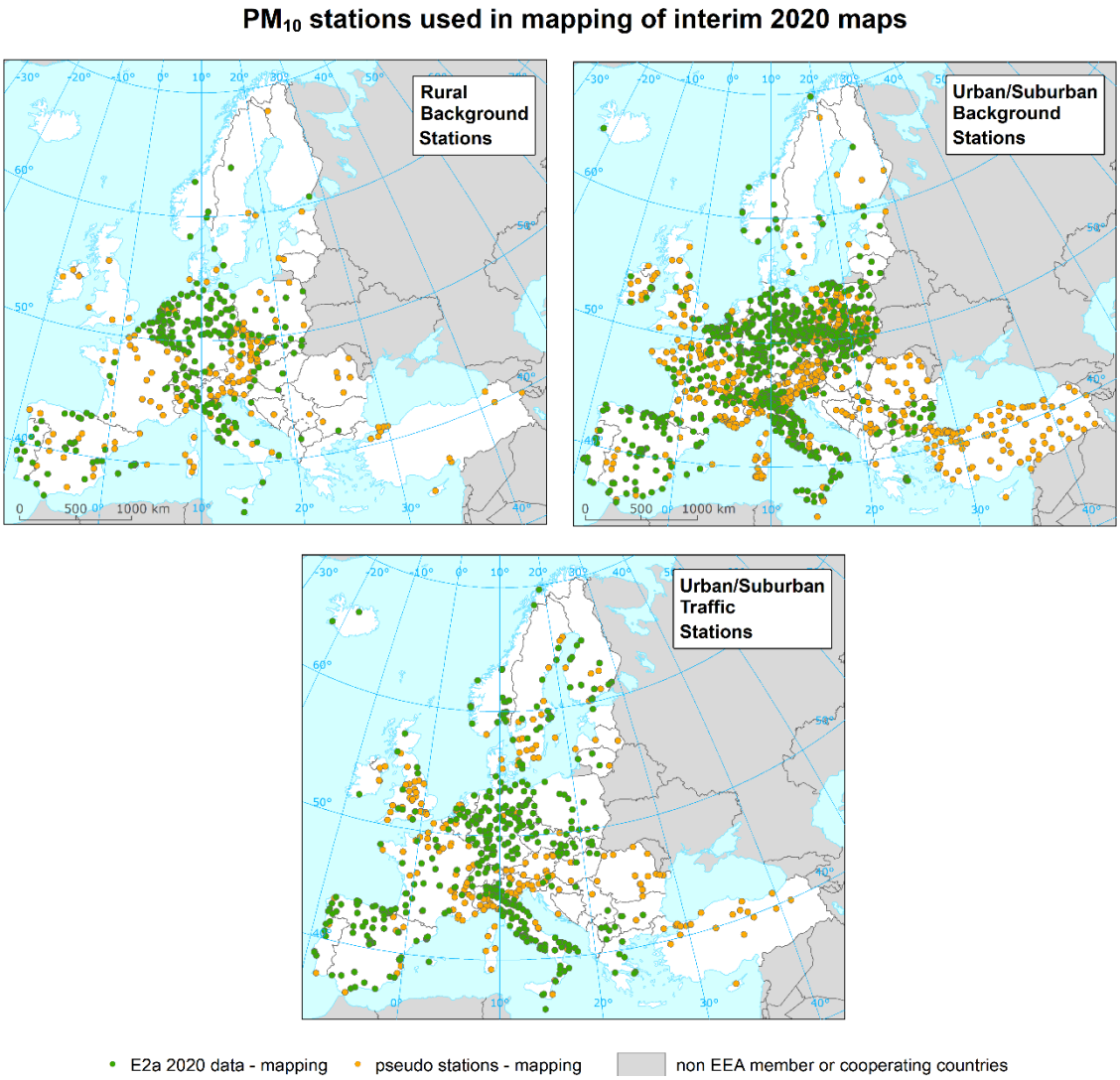

Technical details on the mapping and uncertainty estimates

Like in Horálek et al. (2021b), the pseudo stations data have been estimated at first. The estimates have been calculated based on the E1a measurement data for 2019, the CAMS Ensemble Forecast modelling data for 2019 and 2020, and the regression relation with the E2a measurement data for 2020. Table A.1 presents the regression coefficients determined for pseudo stations data estimation, based on the 989 rural and urban/suburban background and 483 urban/suburban traffic stations that have both E1a 2019 and E2a 2020 measurements available (see Section 2.2.1). Next to this, it presents the statistics showing the tentative quality of the estimate.

Table A.1: Parameters and statistics of linear regression model for generation of pseudo PM_{10} data in rural and urban background and urban traffic areas, for PM_{10} annual average 2020

PM_{10}		Rural and urban background areas	Urban traffic areas
Linear regression model (LRM, Eq. 2.4)	c (constant)	1.1	1.0
	a1 (PM_{10} annual mean 2019, E1a data)	0.584	0.640
	a2 (PM_{10} annual mean 2019 * CAMS ratio 2020/2019)	0.289	0.237
	Adjusted R^2	**0.91**	**0.87**
	Standard Error [µg.m^{-3}]	**1.8**	**2.3**

Based on the E2a data and pseudo data, CAMS Ensemble Forecast modelling data and other supplementary data as used in the regular mapping, the interim PM_{10} annual average map for 2020 has been created. Table A.2 presents the estimated parameters of the linear regression models (*c, a_1, a_2,…*) and of the residual kriging (*nugget, sill, range*) and includes the statistical indicators of both the regression and the kriging of its residuals.

Table A.2: Parameters and statistics of linear regression model and ordinary kriging in rural, urban background and urban traffic areas for interim map of PM_{10} annual average 2020

PM_{10}		Annual average		
		Rural areas	Urban b. areas	Urban tr.. areas
Linear regresion model (LRM, Eq. 2.1)	c (constant)	0.97	0.98	1.63
	a1 (log. CAMS-ENS FC model)	0.783	0.80	0.604
	a2 (altitude GMTED)	-0.00013		
	a3 (relative humidity)	-0.03272		
	a4 (wind speed)	n.sign.		-0.036
	a5 (land cover NAT1)	-0.0017		
	Adjusted R^2	**0.66**	**0.44**	**0.50**
	Standard Error [µg.m^{-3}]	**0.22**	**0.28**	**0.24**
Ordinary kriging (OK) of LRM residuals	nugget	0.019	0.023	0.022
	sill	0.043	0.046	0.039
	range [km]	1000	130	390
LRM + OK of its residuals	**RMSE [µg.m^{-3}]**	**2.7**	**3.6**	**5.1**
	Relative RMSE [%]	**19.1**	**18.8**	**25.5**
	Bias (MPE) [µg.m^{-3}]	**-0.1**	**0.1**	**-0.1**
	R^2 of cross.-val. regr. equation	**0.74**	**0.66**	**0.55**
	Slope of cross-val. regr. equation	**0.72**	**0.72**	**0.55**
	Intercept of cross-val. regr. equation	**3.9**	**5.5**	**8.9**

The Table A.2 shows that the uncertainty of the interim map of PM_{10} annual average expressed by RMSE is about 3 µg·m^{-3} for the rural areas, 4 µg·m^{-3} for the urban background areas, and 5 µg·m^{-3} for the urban traffic areas, respectively. The relative mean uncertainty (Relative RMSE) of this map is 19.1 % for rural areas, 18.8 % for urban background areas, and 25.5 % respectively. However, these uncertaity estimates are valid only for areas covered by the E2a stations. The complete validation of the interim PM_{10} map including the areas not covered by the E2a data can be done when the validated E1a data for 2020 are available.

A.2 NO_2

Maps of measurement stations used for mapping

Map A.2 shows the spatial distribution of the rural, urban/suburban background and urban/suburban traffic stations used in the interim mapping of NO_2 annual average 2020. Like in the case of PM_{10}, the true stations (in green) and the pseudo stations (in orange) are distinguished.

Map A.2: Spatial distribution of NO_2 stations used in interim mapping, 2020

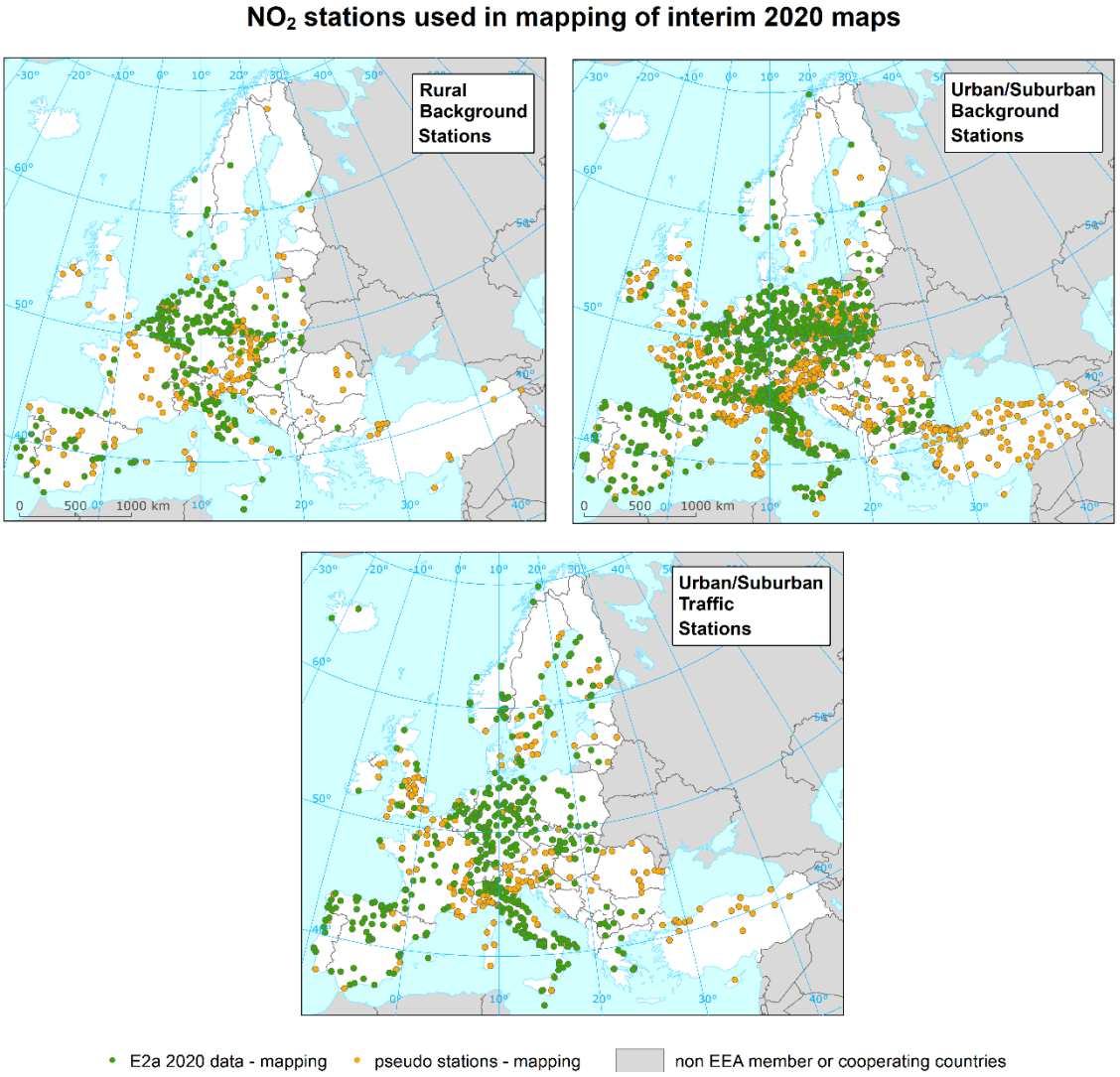

Technical details on the mapping and uncertainty estimates

As a first step for the interim NO_2 annual average 2020 map creation, the pseudo stations data have been estimated, based on the E1a measurement data for 2019, the CAMS Ensemble Forecast modelling data for 2019 and 2020, and the regression relation with the E2a measurement 2020 data. Table A.3 presents the regression coefficients determined for pseudo stations data estimation, based on the 1397 rural and urban/suburban background and 670 urban/suburban traffic stations that have both E1a 2019 and E2a 2020 measurements available (see Section 2.2.1). Apart from this, it gives the statistics showing the tentative quality of the estimate.

Table A.3: Parameters and statistics of linear regression model for generation of pseudo NO_2 data in rural and urban background and urban traffic areas, for NO_2 annual average 2020

NO_2		Rural and urban background areas	Urban traffic areas
Linear regression model (LRM, Eq. 2.4)	c (constant)	0.7	1.4
	a1 (NO_2 annual mean 2019, E1a data)	0.582	0.589
	a2 (NO_2 annual mean 2019 * CAMS ratio 2020/2019)	0.229	0.177
	Adjusted R^2	**0.89**	**0.89**
	Standard Error [µg.m^{-3}]	**2.3**	**2.9**

Based on the E2a data and pseudo data, CAMS Ensemble Forecast modelling data and other supplementary data as used in the regular mapping, the interim NO_2 annual average map for 2020 has been created. Table A.4 presents the estimated parameters of the linear regression models (*c, a_1, a_2,…*) and of the residual kriging (*nugget, sill, range*) and includes the statistical indicators of both the regression and the kriging of its residuals.

Table A.4: Parameters and statistics of linear regression model and ordinary kriging in rural, urban background and urban traffic areas for interim map of NO_2 annual average 2020

NO_2		Annual average		
		Rural areas	Urb. b. areas	Urb. tr. areas
Linear regresion model (LRM, Eq. 2.1)	c (constant)	4.7	13.1	19.03
	a1 (CAMS-ENS-FC model)	0.499	0.217	0.234
	a6 (satellite Sentinel-5P)	0.90	1.515	1.391
	a2 (altitude)	-0.0060	*n.sign.*	*n.sign.*
	a3 (altitude_5km_radius)	0.0054	*n.sign.*	*n.sign.*
	a4 (wind speed)	-0.68	-1.640	-1.401
	a7 (population*1000)	0.00074	0.00019	
	a8 (NAT_1km)		-0.0469	
	a9 (AGR_1km)		-0.0307	
	a10 (TRAF_1km)		0.0654	
	a11 (LDR_5km_radius)	0.0420	*n.sign.*	0.0012
	a12 (HDR_5km_radius)		0.0845	0.0025
	a13 (NAT_5km_radius)	-0.0227	0.46	
	Adjusted R^2	**0.76**	**0.46**	**0.36**
	Standard Error [µg.m^{-3}]	**2.1**	**4.9**	**7.0**
Ordinary kriging (OK) of LRM residuals	nugget	1	11	27
	sill	4	416	37
	range [km]	9	290	80
LRM + OK of its residuals	**RMSE [µg.m^{-3}]**	**1.9**	**4.0**	**6.1**
	Relative RMSE [%]	**28.4**	**26.4**	**25.5**
	Bias (MPE) [µg.m^{-3}]	**0.0**	**0.0**	**-0.1**
	R^2 of cross.-val. regr. equation	**0.80**	**0.57**	**0.52**
	Slope of cross-val. regr. equation	**0.80**	**0.58**	**0.53**
	Intercept of cross-val. regr. equation	**1.4**	**6.1**	**11.3**

The Table A.4 shows that the uncertainty of the interim map of NO_2 annual average expressed by RMSE is about 2 µg·m^{-3} for the rural areas, 4 µg·m^{-3} for the urban background areas, and 6 µg·m^{-3} for the urban traffic areas, respectively. The relative mean uncertainty (Relative RMSE) of this map is 28 % for rural areas, 26 % for urban background areas, and 26 % for urban traffic areas, respectively. However, like for PM_{10}, these uncertainty estimates are valid only for areas covered by the E2a stations. The complete validation of the interim NO_2 map including the areas not covered by the E2a data can be done when the validated E1a data for 2020 are available.

A.3 Ozone

Maps of measurement stations used for mapping

Map A.3 shows the spatial distribution of the rural and urban/suburban background stations used in the interim mapping of O_3 annual average 2020.

Map A.3: Spatial distribution of O_3 background stations used in interim mapping, 2020

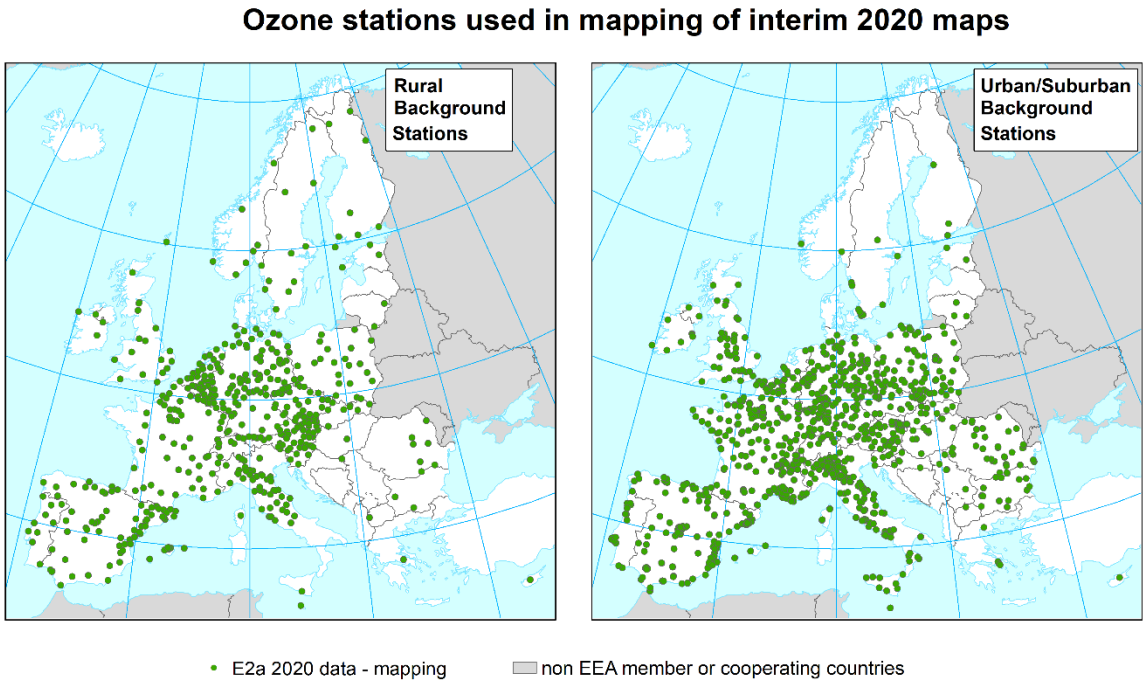

Technical details on the mapping and uncertainty estimates

At first, based on the recommendation of Horálek et al. (2021b) to use pseudo stations only until the data coverage of the E2a data is large enough for construction of the map without such stations, we have checked both the E2a coverage and the quality of a potential pseudo station data estimate. From Map A.3 one can see quite complete spatial coverage of the E2a data, better than in 2019 (Horálek et al., 2021b). Next to this, regression relation (based on the 1501 rural and urban/suburban background stations that have both E1a 2019 and E2a 2020 measurements available) for the potential pseudo data estimates shows R^2 of 0.70 only, which is too week. Thus, we decided not to use the pseudo stations for the ozone interim map construction.

Based on the E2a data, CAMS Ensemble Forecast modelling data and other supplementary data as used in the regular mapping, the interim map of the ozone indicator SOMO35 for 2020 has been created. Due to the increasing data coverage of the E2a data and the weak estimate of the potential pseudo data (R^2= 0.70 only), we have not used the pseudo data.

Table A.5 presents the estimated parameters of the linear regression models (*c, a_1, a_2,…*) and of the residual kriging (*nugget, sill, range*) and includes the statistical indicators of both the regression and the kriging of its residuals, for both map variants.

Table A.5: Parameters and statistics of linear regression model and ordinary kriging in rural and urban background areas for interim map of ozone indicator SOMO35 for 2020

Ozone		SOMO35	
		Rural areas	Urban areas
Linear regresion model (LRM, Eq. 2.1)	c (constant)	-159	1605
	a1 (CAMS-ENS-FC model)	0.96	0.79
	a2 (altitude GMTED)	2.21	
	a3 (wind speed)		-380.2
	a4 (s. solar radiation)	*n.sign.*	*n.sign.*
	Adjusted R^2	**0.52**	**0.47**
	Standard Error [µg·m^{-3}·d]	**1412**	**1368**
Ord. krig. (OK) of LRM residuals	nugget	1.2E+06	7.5E+05
	sill	1.7E+06	1.3E+06
	range [km]	340	120
LRM + OK of its residuals	**RMSE [[µg·m^{-3}·d]**	**1305**	**1115**
	Relative RMSE [%]	**26.7**	**26.3**
	Bias (MPE) [µg·m^{-3}·d]	**13**	**9**
	R^2 of cross.-val. regr. equation	**0.59**	**0.64**
	Slope of cross-val. regr. equation	**0.59**	**0.66**
	Intercept of cross-val. regr. equation	**2028**	**1438**

The Table A.5 shows that the uncertainty of the interim map of ozone indicator SOMO35 expressed by RMSE is 1305 µg·m^{-3}·d for the rural areas and 1115 µg·m^{-3}·d for the urban background areas. The relative mean uncertainty (Relative RMSE) of this map is 27 % for rural areas and 26 % for urban background areas. These uncertainty estimates are valid only for areas covered by the E2a stations. The complete validation of the interim ozone map including the areas not covered by the E2a data can be done when the validated E1a data for 2020 are available.

European Topic Centre on Air pollution,
transport, noise and industrial pollution
c/o NILU – Norwegian Institute for Air Research
P.O. Box 100, NO-2027 Kjeller, Norway
Tel.: +47 63 89 80 00
Email: etc.atni@nilu.no
Web : https://www.eionet.europa.eu/etcs/etc-atni

The European Topic Centre on Air pollution, transport, noise and industrial pollution (ETC/ATNI) is a consortium of European institutes under a framework partnership contract to the European Environment Agency.

European Environment Agency
European Topic Centre on Air pollution,
transport, noise and industrial pollution